RICE FIELD INTERPRETATION WITH TEMPORAL SENTINEL-1 SYNTHETIC APERTURE RADAR IMAGE DATA

[1] *Chia-Hao Chang (張家豪)* [2] *Chiou-Shann Fuh (傅楸善)* [2] *Shi-Wei Wang (王熹偉)*

[1] Dept. of Geography,
[2] Dept. of Computer Science and Information Engineering,
National Taiwan University, Taipei, Taiwan
E-mail: d05228003@ntu.edu.tw, fuh@csie.ntu.edu.tw, swang200207@yahoo.com

ABSTRACT

Rice is the most important crop in Taiwan. Every year, the Agriculture and Food Agency (AFA) has spent lots of budget to monitor or develop efficiently interpretation method the distribution of rice fields. Because Taiwan is a cloudy country, optical remote sensing usually cannot get enough cloud free image in the appropriate time to cover all rice plant area. In this paper, according to Synthetic Aperture Radar (SAR) data can pass through cloud, and the European Space Agency (ESA) has open Sentinel-1 C-Band SAR data to registers for free, we apply spatial-temporal Sentinel-1 data and Local Binary Pattern (LBP) to develop a Rice Fields Temporal LBP Interpretation Method (R-TLIM). By using R-TLIM, the accuracy in overall and producer are 83.55% and 57.82% verify with all ground truth fields polygons. Verify with those polygons are greater than 14m in width, the accuracy in overall and producer are 76.87% and 60.86%.

Keywords *Rice Field Interpretation; European Space Agency (ESA); Sentinel-1; Local Binary Pattern (LBP);* Rice Fields Temporal LBP Interpretation Method (R-TLIM)

1. INTRODUCTION

Remote Sensing data have been widely used to monitor land cover and land use in large area, such as crop's distribution and health conditions. In Taiwan, the Agriculture and Food Agency (AFA) use annually two times of aerial photo to monitor rice distribution in 1st and 2nd rice season. Besides, researchers are also using different remote sensing data to develop more efficiently methods to monitor rice crop fields and estimate production. Chu et al. based on the rice crop's life cycle information in different county of Taiwan, using multi-temporal optical images (such as SPOT series, Formosat-2, aerial or UAV images), analyze with a hybrid classification which integrating iterative self-organizing data. analysis technique algorithm (ISODATA), maximum likelihood classification (MLC), interpretation error analysis and man-machine interaction interpretation, the producer accuracy of rice crop interpretation can up to 95% (Chu et al., 2002, Chu et al., 2003, Chu et al., 2004, Chu et al., 2005, Chu et al., 2006, Chu et al., 2007). Cheng et al. using RADARSAT-2 C-Band quad-polarized SAR images acquired from March to August 2009 to analyze polarimetric response of rice crop field with four-component scattering decomposition (Y4R), including surface scattering, volume scattering, double bounce, and helix scattering. Consider as feature vector, Cheng et al. using CFAR detector to trace the growth stage of rice crop (Cheng et al., 2012).

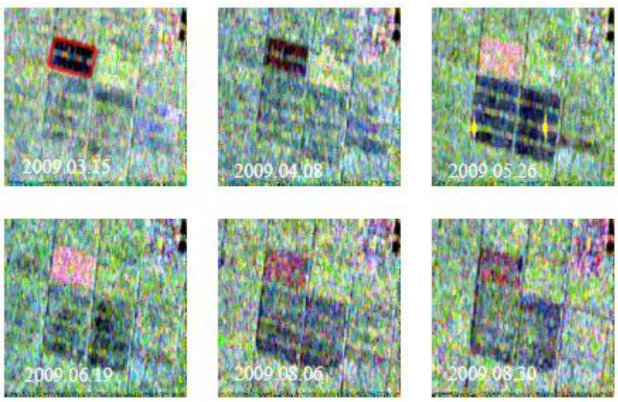

Fig. 1: Different rice crop stages of four-component scattering decomposition. (R:P_d, G:P_v, B:P_s)

Chu et al. using ALOS-1 PALSAR data acquired in 8th April 2011, decomposed polarimetric response with Pauli basis, Y4R, and HH-VV, then classified by minimum distance classification (MDC) and verified with ground truth of 1st rice season in the Yulin County, 2011. The highest rice producer accuracy is HH-VV 91.11%, but the highest overall accuracy is Pauli basis 76.62% (Chu et al., 2014).

Table 1: Interpretation accuracy of Pauli Basis, Y4R, HH-VV decomposition.

	Pauli Basis	Y4R	HH-VV
Producer of Rice	91.01%	85.39%	91.11%
Overall	76.62%	66.88%	70.32%

Chu et al. use temporal Sentinel-1 backscattering data to analyze the difference between rice, building, betel nut, bare soil, and banana. The backscattering is obviously lower the other land cover during transplant (Chu et al., 2016).

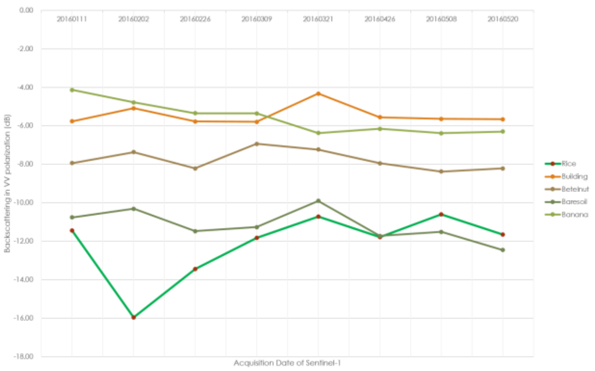

Fig. 2: Temporal backscatter change between different land cover.

From 2014, the European Space Agency (ESA) launched a series of satellites called "Sentinel", including optical and SAR instruments. Monitoring targets are land cover, ocean surface, temperature and atmosphere quality. Most of Sentinel satellite data are open to registers for free. It means anyone who is interested in environmental issues and want to use satellite images to monitor land use or land cover situation can get various image data for those issues. In the series of Sentinel satellite plans, Sentinel-1 plan is a C-Band (5.405 GHz center frequency) Synthetic Aperture Radar (SAR) with single polarization (HH or VV) and dual polarization (HH+HV or VH+VV), which have twin satellites named Sentinel-1A and Sentinel-1B. The orbit height is 700km and 12-days revisit in the same track and same direction. Because SAR system is a positive remote sensing system can operate during day or night. Besides, the operating wavelengths (C-Band) is not impeded by cloud cover, Sentinel-1 can acquire land cover data under all weather conditions. Sentinel-1 have four exclusive acquisition modes: Stripmap (SM), Interferometric Wide swath (IW), Extra-Wide swath (EW) and Wave (WV). To prevent satellite resources conflict, the primary modes are IW, with VV+VH polarization over land, and WV, with VV polarization over open ocean.

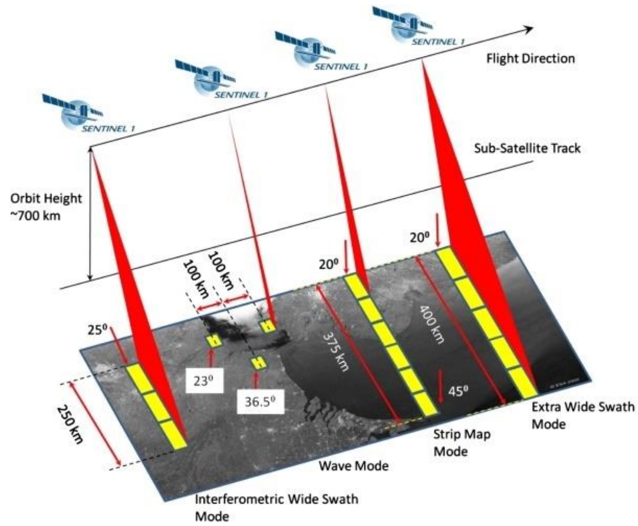

Fig. 3: Acquisition mode of Sentinel-1.

Table 2: The primary conflict-free acquisition modes of Sentinel-1

Mode	Polarization	Main Targets
IW	VV+VH	land
WV	VV	open ocean
EW	----	wide area coastal, oil spill, sea-ice
SM	----	Extraordinary events

In 1994, Ojala et al. based on the contract between pixel and eight neighbors, developed a locally texture description method, Local binary Pattern (LBP) operator. In the beginning, LBP use the sign of eight differences between central and neighbors, recorded into an 8-bit number (Ojala et al., 1996, Ojala et al., 2001).

$$\mathrm{LBP} = \sum_{i-1}^{8} s(g_0, g_i)2^{i-1}, \qquad s(g_0, g_i) = \begin{cases} 1, if\ g_i \geq g_0, \\ 0, if\ g_i < g_0. \end{cases}$$

2. METHODOLOGY

Although LBP is an efficient method use to descript local texture in 2D images. But for locally homogenous land cover type, such as water body, rice fields, grassland, and flat bare land, the separability of LBP is not explicit. Because the agricultural land cover is change with crop's lifecycle, image patterns in the remote sensing data are changed also. In this paper, by using time series of Sentinel-1 IW mode SLC image data to avoid the cloud cover influence, applying LBP operator into temporal backscatter change of SAR images, we analyze rice crop's backscatter change pattern in 1st rice season 2016.

After define the rice crop's backscatter change pattern, we calculate all pixel's LBP and filter out the rice pixels. Finally, by using ground truth field polygons, we verify the interpretation accuracy of rice fields.

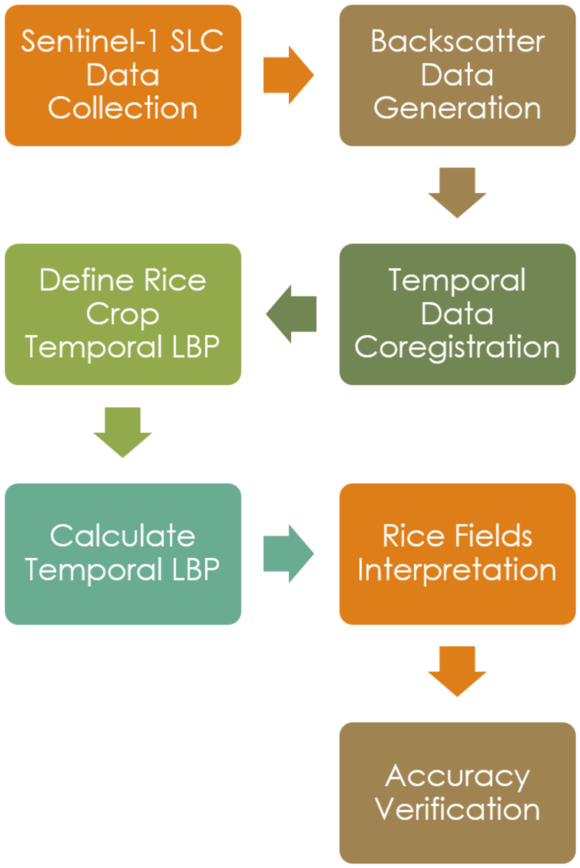

Fig. 4: Research flow of rice fields' interpretation with temporal LBP

3. DATA

3.1. Farm Field Polygons and Ground Truth Data

We use farm field polygons data to calculate LBP, interpret rice pixel and use rice distribution polygons data to verify the accuracy. These data are provided by AFA and produced during 1st rice season, 2016.

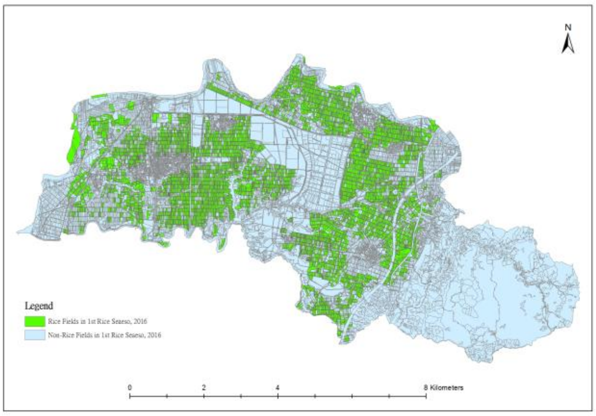

Fig. 5: Farm field and ground truth polygons data in Liouying District.

3.2. Sentinel-1 SLC Image Data

We collected Sentinel-1 SLC image data for each month from 11th Jan to 12th Dec in 2016. To avoid the potential polarimetric response error from different acquire direction and satellite obits, all image data are cover southern Taiwan in the same orbit with descending direction.

Table 3: Image data of Sentinel-1

Date		Orbit	Mode	Level	Swath
11th Jan.	21th Jul.	215	IW	SLC	IW2
4th Feb.	14th Aug.				
23th Mar.	7th Sep.				
16th Apr.	1st Oct.				
10th May	18th Nov.				
3rd Jun.	12th Dec.				

4. RESULTS AND DISCUSSION

4.1. SAR Image Pre-processing

Because of the Liouying District, Tainan County is located in the second swath of SAR image data used in this paper, we only processed these swaths of SAR SLC image data into backscatter image. The backscatter image process sequence via ESA SNAP are shown in Fig. 1. Fig. 2 shows single swath data of SLC image, GRD image and backscatter feature image of 4th Feb. 2016.

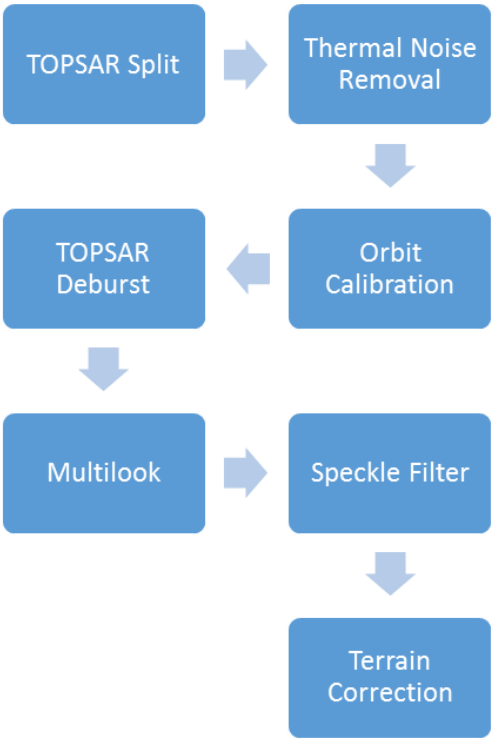

Fig. 6: Process sequence of SLC to GRD image.

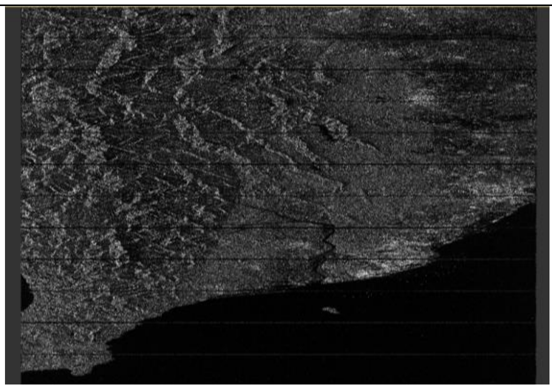

(a) Single swath data of SLC image.

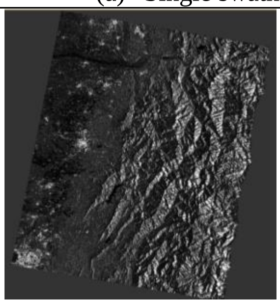

(b) GRD image.

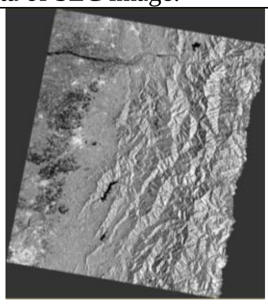

(c) Backscatter image.

Fig. 7: Sample image of SLC, GRD and Backscatter (4th Feb. 2016).

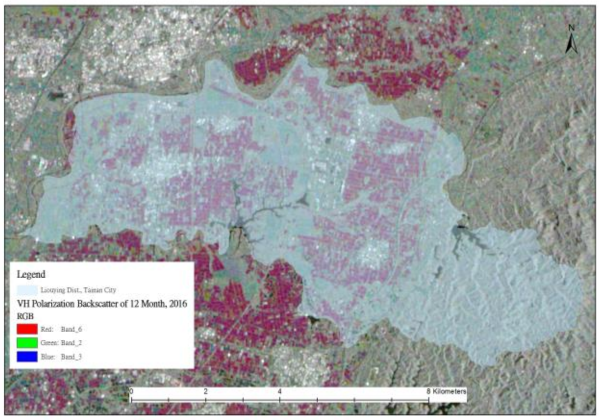

(a) Combination of 12 backscatter images in VH polarization. (R: Jun., G: Feb., B: Mar.).

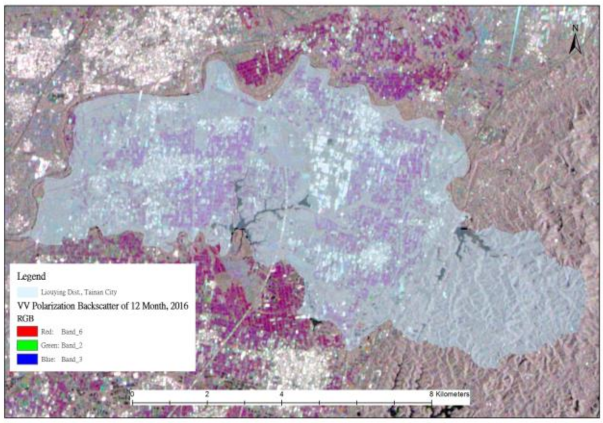

(b) Combination of 12 backscatter images in VV polarization. (R: Jun., G: Feb., B: Mar.).

Fig. 8: Backscatter images combination and overlap with Liouying District.

4.2. Temporal LBP Calculation

Rice crops are relatively homogeneous within fields in SAR image at single time period, so that LBP cannot separate rice from other land cover types correctly. Because the backscatter feature of rice is changed with the stage of rice crop's life cycle, we apply LBP into monthly backscatter temporal change feature with rice fields.

Farmers mostly start to transplant rice in January in Liouying District, so that the backscatter feature are similar to water body in February. In this paper, we set the backscatter feature of February as base line, compare the backscatter feature from March to October at the same location and calculate temporal LBP.

Because the digital number of backscatter are negative number and save in 32bit floating format, to reduce the complexity during LBP calculation, all pixels are plus 100 and saved into 8bit integer format before calculating temporal LBP. Although temporal pixel value are different from VH and VV polarization, but the temporal change of sign are almost the same. So that the temporal LBP distribution pattern of VH and VV polarization are quite similar.

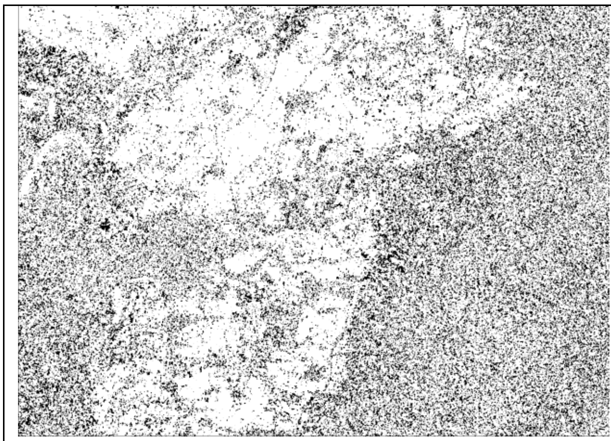

(a) Temporal LBP of VH polarization.

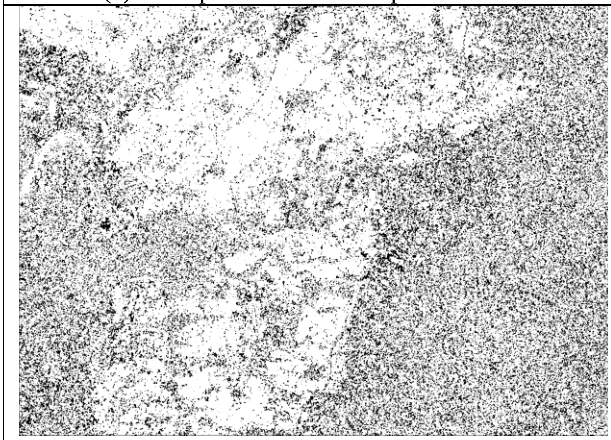

(b) Temporal LBP of VV polarization.

Fig. 9: Temporal LBP distribution pattern of VH and VV polarization

4.3. Threshold of Rice Pixel

To understand the temporal LBP of rice pixel, we subset three different image chips of rice growing area around Liouying District with VH and VV polarization backscatter. Then we calculate temporal LBP and statistics of these three rice image chips. With statistics, except the average of Sample 2 in VV polarization is obviously lower than others, the average are higher than 189.

Table 4: Statistics of rice fields image chips.

	Rice 1		Rice 2		Rice 3	
	VH	VV	VH	VV	VH	VV
Average	203.87	189.76	198.87	142.09	204.26	214.37
STD.	13.51	29.64	20.82	29.27	11.51	8.13

The 1st rice season in Liouying District mostly starts to transplant rice in January and harvester in June. Fields would lay bare or fallowed during later June to later July or early August then plant 2nd season crop. It means that backscatter feature is getting stronger from February to June. After 1st rice harvester, backscatter would decrease but still higher than transplant period. Table 2 shows temporal LBP with different agriculture behaviors in the rice fields. According to Table 2, we define the rice temporal LBP threshold as 200.

Table 5: Sample of temporal LBP in rice pixel.

	Month									LBP
	2	3	4	5	6	7	8	9	10	Sum.
LBP	0	1	1	1	1	1	0	1	1	223
	0	1	1	1	1	0	1	1	1	239
	0	1	1	1	1	1	1	1	1	255
Ag. type	Rice in 1st Season					Rice or other in 2nd Season				

4.4. Rice Field Interpretation

With the temporal LBP threshold of rice pixel, we classify all image pixel into rice or non-rice. Then we use Zonal Statistic Function in ESRI ArcGIS to calculate the majority pixel class in each ground truth field polygon and define the field type by the majority class.

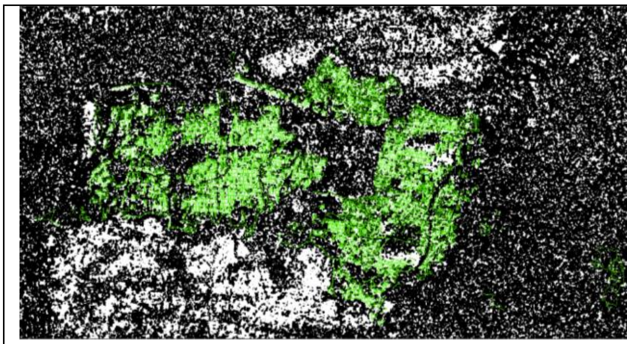

(a) Rice Interpretation of VH polarization overlap ground truth rice polygons.

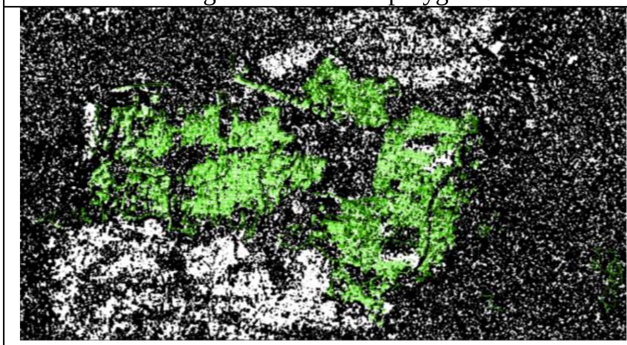

(b) Rice Interpretation of VV polarization overlap ground truth rice polygons.

Fig. 10: Rice Interpretation of VH and VV polarization

Compare the interpretation results of VH and VV polarization, because the backscatter of 4th Feb. are the lowest in VH and VV polarization during 1st rice season, the temporal LBP and rice field interpretations are the same between VH and VV polarization.

Table 6: Comparison between VH and VV rice interpretations.

		Ground Truth			
		Rice	Non-Rice	Total	U.A.
Classified	Rice	7964	0	7964	100.00%
	Non-Rice	0	33474	33474	100.00%
	Total	7964	33474	41438	
	P.A.	100.00%	100.00%	**Overall**	**100.00%**
				kappa	1.00

The rice field interpretation result is verify with ground truth field polygons. The overall accuracy is 83.55%, but producer accuracy of rice is only 57.82%. The distribution is show in Fig. 11. Some of non-rice fields with similar temporal LBP is error classified as rice fields, such as eastern-southern part of Liouyin Dist. (Fig. 12).

Table 7: Accuracy with all ground truth polygons.

		Ground Truth			
		Rice	Non-Rice	Total	U.A.
Classified	Rice	4245	3719	7964	53.30%
	Non-Rice	3097	30377	33474	90.75%
	Total	7342	34096	41438	
	P.A.	57.82%	89.09%	**Overall**	**83.55%**
				kappa	0.45

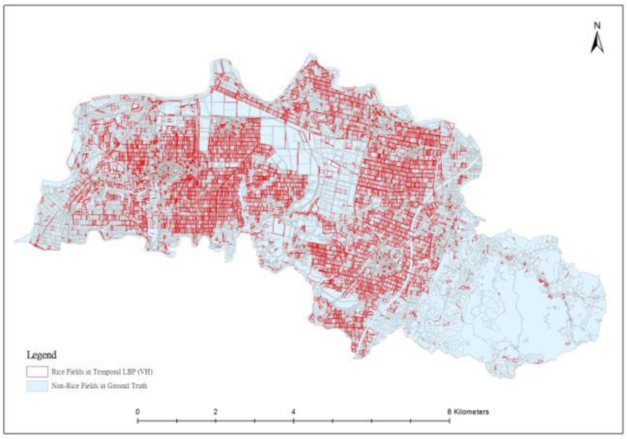

Fig. 11: Rice fields distribution of VH polarization.

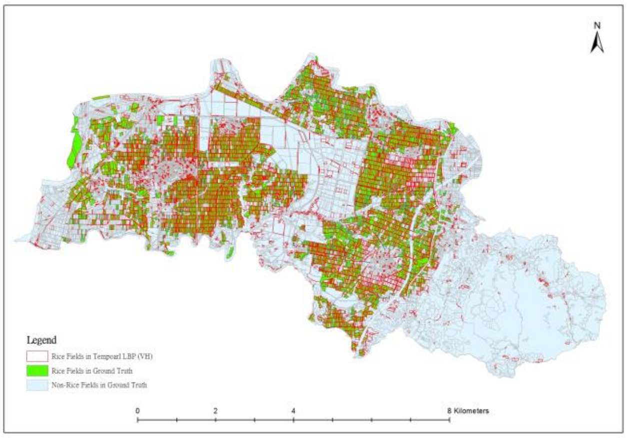

Fig. 12: Rice fields distribution of ground truth and VH polarization.

Because some fields are too thin for Sentinel-1 image data, we use 7m inner buffer to filter out those field polygons which are not wider than 14m. After that, we verify with those ground truth polygons wider than 14m and accuracy in overall and producer are 78.87% and 60.86%. The distribution is show in Fig. 13. There are still some non-rice fields with similar temporal LBP is error classified as rice fields (show in Fig. 14).

Table 8: Accuracy with ground truth polygons wider than 14m.

		Ground Truth			
		Rice	Non-Rice	Total	U.A.
Classified	Rice	3682	1390	5072	72.59%
	Non-Rice	2368	8810	11178	78.82%
	Total	6050	10200	16250	
	P.A.	60.86%	86.37%	**Overall**	**76.87%**
				kappa	0.49

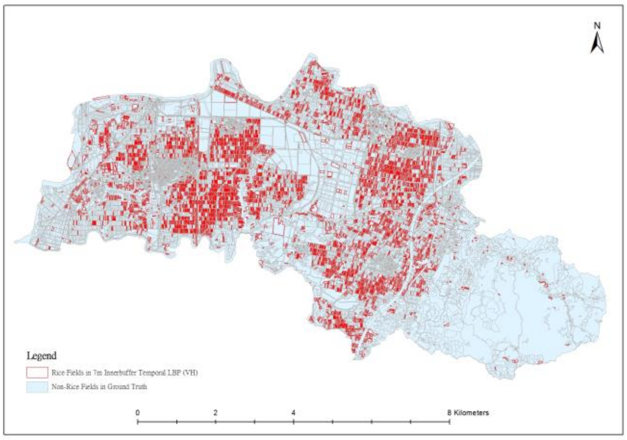

Fig. 13: Rice fields distribution of VH polarization with 7m inner buffer.

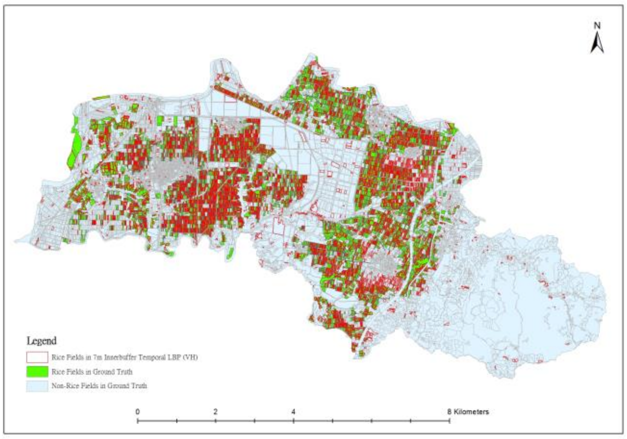

Fig. 14: Rice fields distribution of ground truth and VH polarization with 7m inner buffer.

Compare with original and filter by 7m inner buffer interpretation results, error classified fields located in building area and along with road are mostly been filtered out, e.g. the red polygons show in Fig. 15. But some error classified fields still there, such as some light blue polygons with red boundary in the middle part of Liouying Dist. (Fig. 14).

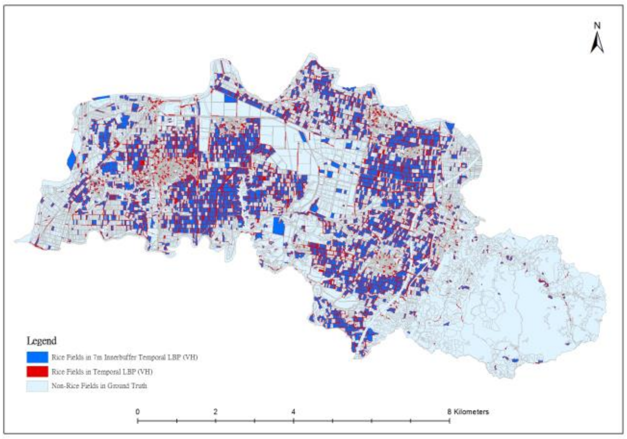

Fig. 15: Rice fields distribution of VH polarization and VH polarization with 7m inner buffer.

5. CONCLUSION

In this paper, we demonstrate rice fields can be interpreted by temporal backscatter image of SAR with LBP. The overall accuracy is from 76.87% to 83.55%, but from 57.82% to 60.86% in producer accuracy of rice fields. Because we only use temporal LBP to interpret rice field's polygon, some non-rice fields with similar temporal LBP are error classified. It could be decrease the number of these kind of error by consider the threshold of LBP and the variance of temporal backscatter change.

The shape of rice fields are mostly in narrow rectangle in Taiwan. Part of those rice fields are too thin for SAR image. It could be one possible reason of lower producer accuracy in rice fields.

Taiwan is in a cloudy area. Although the rice fields producer accuracy can higher than 96% with optical remote sensing data and analyze techniques, but still cannot interpret the cloud cover area. SAR is a positive remote sensing technique can provide land cover information over day and night regardless cloud cover. Based on our results, an efficient rice field's interpretation method with temporal SAR data and LBP is proposed. It can be focus upon develop interpret methods of different land cover type, over season's lifecycle changing pattern of rice fields, integrate optical image data to improve the interpretation accuracy.

REFERENCES

[1] T. Y. Cheng, C. Y. Chu, K. S. Chen, Y. Yamaguchi, S. J. Lee, "Time Series SAR Polarimetric Analysis of Rice Crop based on Four-Component Scattering Decomposition", ISAP2012, pp.620-623, 2012

[2] C. H. Chu, K. C. Chang, R. Y. Lee, "Applying High Satellite Imagery to assist farming inventory (I)", Agriculture and Food Agency, 2002

[3] C. H. Chu, K. C. Chang, R. Y. Lee, "Applying High Satellite Imagery to assist farming inventory (II)", Agriculture and Food Agency, 2003

[4] C. H. Chu, K. C. Chang, R. Y. Lee, "Applying High Satellite Imagery to assist farming inventory (III)", Agriculture and Food Agency, 2004

[5] C. H. Chu, C. C. Liu, Y. S. Tseng, T. Y. Chou, "The Application on Investigation of Rice Field Using the High Frequency and High Resolution Satellite Images (1/3)", Agriculture and Food Agency, 2005

[6] C. H. Chu, C. C. Liu, Y. S. Tseng, C. C. Lei, "The Application on Investigation of Rice Field Using the High Frequency and High Resolution Satellite Images (2/3)", Agriculture and Food Agency, 2006

[7] C. H. Chu, C. C. Liu, Y. S. Tseng, C. C. Lei, "The Application on Investigation of Rice Field Using the High Frequency and High Resolution Satellite Images (3/3)", Agriculture and Food Agency, 2007

[8] C. H. Chu, et al., "Study on Applying High Resolution Optical Satellite Image and L-Band SAR Image to Crops Production Investigation and Reexamine Mechanism" , Agriculture and Food Agency, 2014

[9] C. H. Chu, et al., "Research of Apply UAV, Remote Sensing Information and Multi-Scale Spatial Information Transform Classification Model to Improve Paddy Rice Area and Yields Investigation Technique" , Agriculture and Food Agency, 2016

[10] F. De Zan, A. M. Guarnieri, “TOPSAR: Terrain Observation by Progressive Scans”, Geoscience and Remote Sensing, IEEE Transactions on, 44(9), pp.2352–2360, 2006

[11] T. Ojala, M. Pietikäinen, D. Harwood, A comparative study of texture measures with classification based on featured distributions, Pattern Recognition, 29(1): 51-59, 1996.

[12] T Ojala, K Valkealahti, E Oja, M Pietikäinen, Texture discrimination with multidimensional distributions of signed gray-level differences, Pattern Recognition, Pattern Recognition, 34, pp.727-739, 2001.

[13] ESA Sentinel Online （https://sentinel.esa.int/web/sentinel/home）